Astronomy
&
Astrophysics

Element abundances in cool white dwarfs

II. Ultraviolet observations of DZ white dwarfs[*]

B. Wolff[1], D. Koester[1], and J. Liebert[2]

[1] Institut für Theoretische Physik und Astrophysik, Universität Kiel, 24098 Kiel, Germany
    e-mail: koester@astrophysik.uni-kiel.de
[2] Steward Observatory, University of Arizona, 933 North Cherry Avenue, Tucson, AZ 85721, USA
    e-mail: liebert@as.arizona.edu

Abstract. We present a small data base of homogeneously derived photospheric element abundances of DZ white dwarfs and related objects. Our previous investigations are supplemented with the analysis of ultraviolet spectra for nine white dwarfs. Of particular interest is the detection of Lα absorption in van Maanen 2 and a determination of the effective temperature of this star. The new value is about 1000 K lower than previous results due to the strong ultraviolet absorption by metals which has to be considered consistently. The metal abundances of our sample stars are compatible with the predictions from the two-phase accretion model of Dupuis et al. (1992, 1993a, 1993b). Small deviations can be observed for the abundance ratios in some objects. This could indicate non-solar metal-to-metal ratios in the accreted material. Hydrogen can be detected in virtually all of our objects. However, its average accretion rate must be at least two orders of magnitude lower than the metal accretion rate.

Key words. stars: abundances – stars: atmospheres – white dwarfs – ultraviolet: stars

1. Introduction

At the cool end of the white dwarf sequence traces of heavier elements can be found in several objects with hydrogen- and helium-rich atmospheres. The presence of metals is usually attributed to accretion from denser parts of the interstellar medium combined with diffusion into deeper layers. This idea has been put on a sound theoretical basis by Dupuis et al. (1992, 1993a, 1993b) whose two-phase accretion model assumes that accretion of metals is low ($\dot{M} \approx 5 \times 10^{-20}\ M_\odot\ \mathrm{yr}^{-1}$) most of the time and is larger ($\dot{M} \approx 5 \times 10^{-15}\ M_\odot\ \mathrm{yr}^{-1}$) only during rare and short passages through interstellar clouds. Since the accreted elements diffuse downwards on time scales of typically 10^6 years they are only visible during or shortly after such encounters.

Empirical tests of the accretion model benefit from different diffusion time scales of the elements so that photospheric abundances and abundance ratios vary in a characteristic way with time after the encounter. Dupuis et al. (1993b) concluded that – within the large observational uncertainties – the two-phase accretion model can account for the observed abundances and their ratios. The most notable remaining problem for the helium-rich objects (spectral types DZ and DBZ) is the accretion of hydrogen. As the lightest element, hydrogen is not subject to downward diffusion and should be accumulated in the upper atmospheric layers. However, hydrogen is only rarely observed in DZ stars and the measured abundances are usually rather low.

A general problem of previous comparisons is the uncertainty arising from observations with low signal-to-noise ratios and model atmospheres not including recent advances in input physics. In Paper I (Koester & Wolff 2000), we have concluded that it is worthwhile to study the abundance patterns in DZ white dwarfs again using new or newly calibrated observations and the latest improvements in model atmosphere calculations. The ultimate goal is a homogeneous data base of element abundances for the comparison with the two-phase accretion model.

Table 1. Observations.

WD Number	Name	Observations	$\lambda/$ Å	$\Delta\lambda/$ Å	Remarks
0002+729	GD 408	IUE, SWP19006L	1150–1950	6.0	
		IUE, LWR15058L	1850–3250	6.0	
		MMT	3750–4650	1.0	Sion et al. (1988)
0038−226	LHS 1126	HST/FOS, G190H	1573–2330	1.5	
		HST/FOS, G270H	2221–3301	2.1	
		HST/FOS, G400H	3240–4822	3.1	
		BVRIJHK photometry	4400–22 000		Bergeron et al. (1997)
0046+051	vMa 2	IUE, LWR03322L	1850–3250	6.0	
		IUE, LWR06474L	1850–3250	6.0	
		Calar Alto, 3.5 m	3730–5075	4.0	
		BVRIJHK photometry	4400–22 000		Bergeron et al. (1997)
0552−041	LP 658-2	HST/FOS, G190H	1573–2330	1.5	
		HST/FOS, G270H	2221–3301	2.1	
		HST/FOS, G400H	3240–4822	3.1	
		BVRIJHK photometry	4400–22 000		Bergeron et al. (1997)
0752−676	BPM 4729	HST/FOS, G190H	1573–2330	1.5	
		HST/FOS, G270H	2221–3301	2.1	
		HST/FOS, G400H	3240–4822	3.1	
		BVRIJHK photometry	4400–22 000		Bergeron et al. (1997)
1011+570	GD 303	IUE, SWP18994L	1150–1950	6.0	
		IUE, LWR15047L	1850–3250	6.0	
		MMT	3750–4650	1.0	Sion et al. (1988)
1225−079	K 789-37	IUE, SWP30001L	1150–1950	6.0	
		IUE, LWP09836L	1850–3250	6.0	
		SAAO, 1.9 m	3600–5000	5.0	Koester et al. (1990)
1822+410	GD 378	IUE, SWP19549L	1150–1950	6.0	
		IUE, LWR15578L	1850–3250	6.0	
		MMT	3750–4650	1.0	Sion et al. (1988)
2216−657	L 119-34	IUE, SWP29720L	1150–1950	6.0	
		IUE, LWR14743L	1850–3250	6.0	

We started in Paper I with the Hubble Space Telescope (HST) observations of the DZA white dwarfs L 745-46A and Ross 640. Both objects show weak Balmer lines in addition to metals and are therefore interesting with regard to the hydrogen problem mentioned above. We have used the high quality HST spectra to test our analysis methods and to study the remaining uncertainties of the model atmospheres. In comparison with previous investigations, we were able to determine more accurate element abundances, especially for carbon and iron. Major improvements were possible for the modeling of the broad Lα lines in both stars which could be reproduced for the first time without any unphysical assumptions. This provides new means for the analysis of the hydrogen content in cool white dwarfs.

In this paper, we analyze all available ultraviolet observations of white dwarfs with spectral types DZ and DBZ. The ultraviolet is very suited for the study of metal abundances because the relevant elements have in general much stronger lines in this part of the electromagnetic spectrum than in the optical part – with the exception of the Ca II H and K lines. We use for most stars observations with the International Ultraviolet Explorer (IUE) which have been newly calibrated (NEWSIPS) and which show significant

improvements compared to older versions. HST/FOS observations could also be used for three stars.

2. Model atmospheres

A general description of the procedures used for the calculation of our LTE model atmospheres and synthetic spectra has been given by Finley et al. (1997). Further details can be found in Paper I. We only explain briefly the effects of different equations of states (EOS) and the treatment of Lα absorption.

We use for our models a version of the Hummer-Mihalas-Däppen EOS (Mihalas et al. 1990) which predicts larger non-ideal effects and larger ionization than the EOS by Saumon & Chabrier (1994) and Saumon et al. (1995). In Paper I, we have compared the results of our standard models with models were non-ideal effects are switched off and the ionization fraction is determined only by thermal effects using the unmodified Saha equation. For models with effective temperatures of about 8000 K non-ideal effects are negligible but the situation may be different at the lower temperatures of some of the stars in this paper. We therefore test the influence of non-ideal effects in these cases.
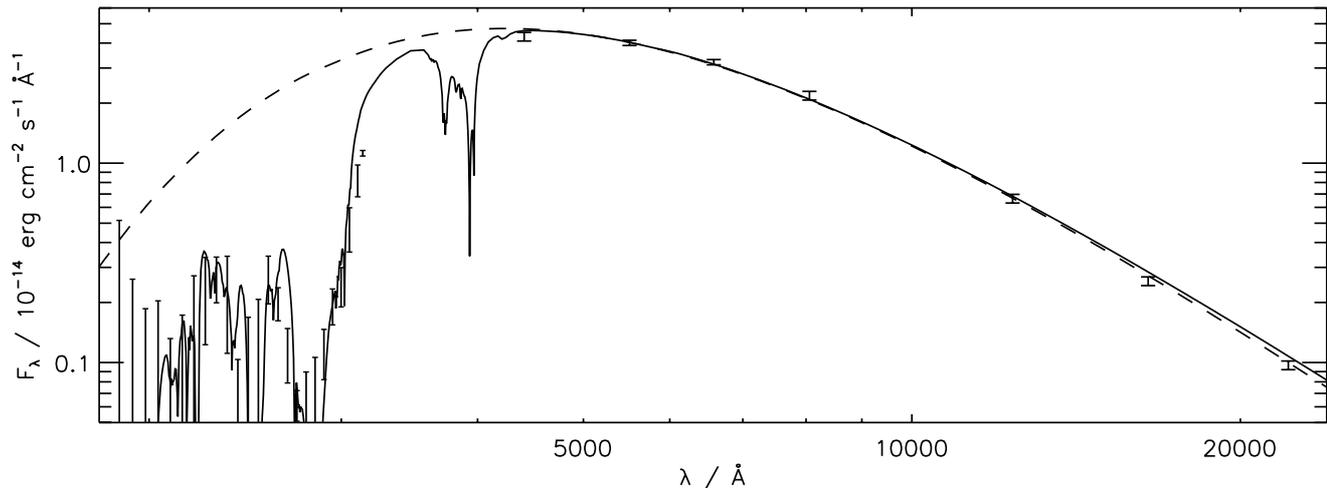
Fig. 1. Flux distribution of van Maanen 2: $BVRIJHK$ photometry from Bergeron et al. (1997) and IUE observations (rebinned to 60 Å resolution). The continuous curve is a model with $T_{\text{eff}} = 5700$ K, metals, and hydrogen, the dashed curve a pure helium model with $T_{\text{eff}} = 6700$ K.

Of importance for the analysis of the HST spectra of L 745-46A and Ross 640 has been the Lα wing which dominates the UV spectra of both stars. Since model calculations using van-der-Waals broadening by neutral helium result in a Lα wing extending far into the optical region we have developed in Paper I a new approach to model this line. Since we are only interested in the far wings we use the quasistatic limit of the broadening theory (see e.g. Allard & Kielkopf 1991) but take into account two effects which are important at high perturber densities: the variation of the transition probability with distance between emitter and perturber and the strongly repulsive potential at close distances. With this procedure we were able to reproduce the Lα wings in both stars at the same abundances as derived from optical Balmer lines.

3. Observations

Three of our objects have been observed with the Faint Object Spectrograph (FOS) onboard HST. For the remaining six DZ/DBZ white dwarfs we have used low dispersion IUE spectra. The IUE data were retrieved from the IUE final archive and have been calibrated with the NEWSIPS calibration (Nichols et al. 1994). In addition to these data, we have also used optical observations and optical photometric scans. A list of the observations can be found in Table 1.

4. Analysis

4.1. Van Maanen 2

Van Maanen 2 (WD 0046+051) is one of the three classic white dwarfs. It is a cool and very metal-rich DZ star, the optical spectrum exhibiting, besides the typical Ca II H+K lines, Ca I at 4227 Å, Fe I at 4384 Å, and several Fe I lines on the blue wing of Ca II. Analysis of this star, using model atmospheres, has been pioneered

by Weidemann (1960) and later by Wegner (1972) and Grenfell (1974). The ultraviolet spectrum is dominated by the strong Mg I line at 2852 Å. Also important are the Mg II lines at 2796/2803 Å and several weak lines of Fe I and Fe II. Until now, the ultraviolet spectrum has not been analyzed in detail. Bergeron et al. (1997, 2001) have recently determined $T_{\text{eff}} = 6770$ K from $BVRIJHK$ photometry using a pure helium atmosphere. Combining this result with the trigonometric parallax they also derived $\log g = 8.40$.

We use the photometry together with the co-added IUE LWR spectra to define the flux distribution of van Maanen 2. An optical spectrum (3730–5075 Å) obtained at the Calar Alto observatory complements the observations for the determination of metal abundances. We started the analysis with a pure helium atmosphere of $T_{\text{eff}} = 6700$ K. Figure 1 shows the fit of this model to the flux distribution. To account for the solid angle of the star the model has been scaled to reproduce the infrared J magnitude. It fits the photometric data well but fails to reproduce the overall flux level at ultraviolet wavelengths where the absorption from metals is important. Then we calculated model atmospheres and spectra with $T_{\text{eff}} = 6700$ K and several chemical compositions to determine the abundances of magnesium, calcium, and iron from optical and ultraviolet lines by a visual comparison. It turned out that the backwarming effect from the ultraviolet absorption – especially from the strong Mg I line – and the effect of increased electron density significantly alter the flux distribution. The effective temperature has to be reduced and, consequently, the abundances have to be determined again. In an iterative process we finally derived $T_{\text{eff}} = 5700$ K, about 1000 K lower than the original result from Bergeron et al.

Figure 1 shows that the new model can account for the complete observed flux distribution. At optical and infrared wavelengths both model spectra are virtually
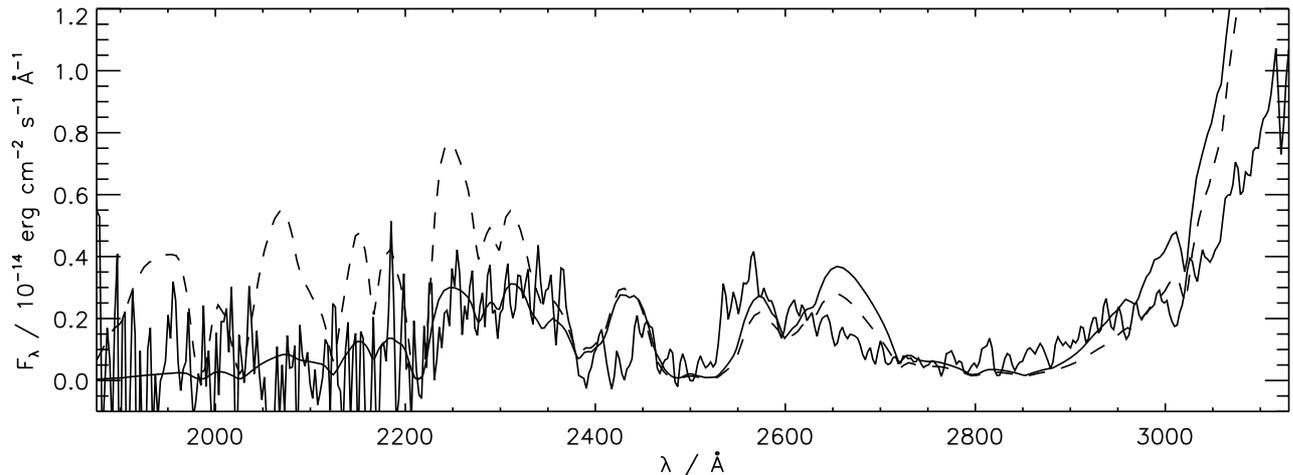
Fig. 2. IUE spectrum of van Maanen 2 compared to a model with $T_{\rm eff} = 5700$ K, $\log g = 7.9$, $\log {\rm H/He} = -5.0$, $\log {\rm Mg/He} = -9.1$, $\log {\rm Si/He} = -9.0$, $\log {\rm Ca/He} = -10.65$, $\log {\rm Fe/He} = -9.4$ (solid line) and a model with the same parameters but without hydrogen (dashed line).

identical. Our effective temperature is similar to previous results from e.g. Wegner (1972), Grenfell (1974), and Liebert et al. (1987) who considered the contributions of metals as electron donators in their calculations. This shows the importance of an accurate chemical composition for determining effective temperatures of DZ white dwarfs and related objects – a result which is also found and discussed in more detail by Provencal et al. (2002) in their analysis of Procyon B.

From a visual comparison of the fits to the flux distribution with different models we estimate the error of $T_{\rm eff}$ to about ± 200 K. The solid angle necessary to reproduce the photometry together with the trigonometric parallax from Hipparcos ($\pi = 226.95 \pm 5.35$ mas; ESA 1997) and the mass-radius relation from Wood (1994; without hydrogen) implies a surface gravity of $\log g = 7.9$. The uncertainties in $T_{\rm eff}$ and π translate into ± 0.2 for the log of the gravity. The higher value of $\log g = 8.4$ derived by Bergeron et al. (1997, 2001) is due to the higher effective temperature which gives a higher intrinsic flux and therefore a smaller radius and a larger mass for the star.

The absorption from magnesium, calcium, and iron alone cannot reproduce the ultraviolet flux completely. As illustrated in Fig. 2, there is a significant discrepancy at $\lambda \lesssim 2300$ Å. We have included in the model calculations all lines from the identified metals and have also determined an upper limit for silicon. One may speculate that other unidentified metals may be responsible for the absorption. However, we do not think this to be plausible since, for example, the absorption from C I at 1930 Å would result in a competely different shape and other metals than the ones considered here have not been observed so far in DZ white dwarfs. With regard to the experience with absorption from Lα in L 745-46A and Ross 640 (Paper I) we would rather attribute the missing opacity to hydrogen. Figure 2 shows that adding an abundance of $\log {\rm H/He} = -5.0$ improves the fit considerably. The Balmer lines are too weak at this abundance to be detected in existing optical spec-

tra so that the analysis of the hydrogen content must rely entirely on Lα.

The results for van Maanen 2 are summarized in Table 2. For the abundances, we include three different error sources: uncertainties from effective temperature, gravity, and from the choice of the equation of state. These systematic effects dominate the total error whereas pure statistical contributions are of minor importance. Formal statistical errors are comparitively low and do not reflect the true uncertainties. Therefore, we have determined the individual contributions from the systematic error sources using visual comparisons to models with different parameters and have added the contributions quadratically. As mentioned in Sect. 2, non-ideal effects are not important in the somewhat hotter stars L 745-46A and Ross 640. However, a weak influence can be observed in van Maanen 2. If we use the Saha equation instead of our standard EOS, then the gas pressure increases whereas the electron density decreases and the absorption lines – especially the wings – are in general somewhat broader. The abundances have to be changed by about 0.1 to 0.2 dex to account for this effect.

4.2. LHS 1126, LP 658-2, and BPM 4729

The analysis of van Maanen 2 shows the importance of the ultraviolet region for the temperature determination and the question of the hydrogen abundance. It seems, therefore, worthwhile to investigate the ultraviolet spectra of other white dwarfs with similar effective temperature. In this section, we present HST/FOS observations of LHS 1126, LP 658-2, and BPM 4729, the coolest white dwarfs in our sample. The observations have been obtained in guaranteed time but have not been published so far since the fluxes differed decisively from the predictions of preexisting models raising some doubts about the accuracy of the FOS calibration. However, without going into details, we consulted with Ronald Downes of the
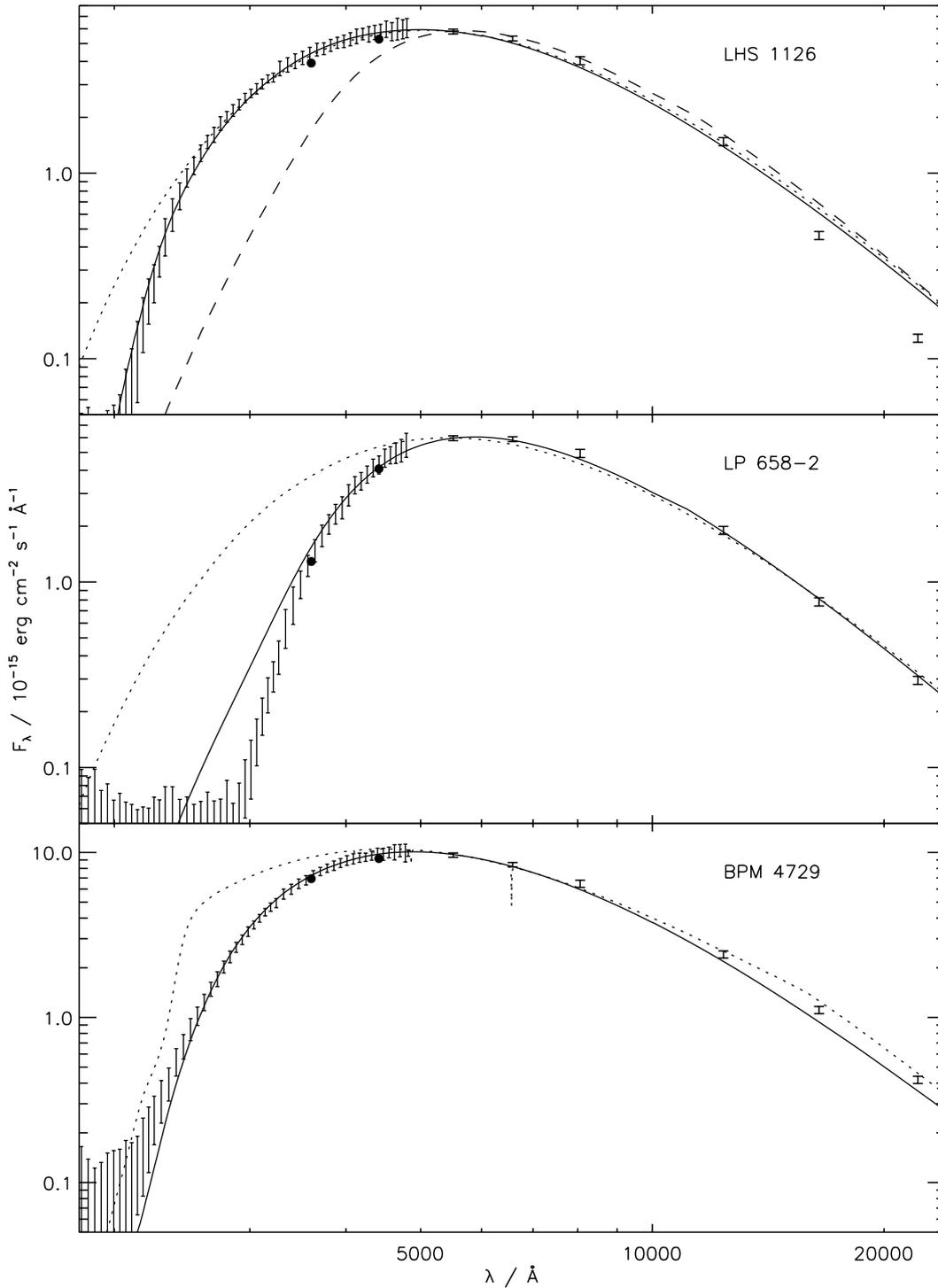
Fig. 3. HST/FOS spectra (bars) of LHS 1126 (top), LP 658-2 (middle), and BPM 4729 (bottom) combined with $VRIJHK$ photometry from Bergeron et al. (2001). Additional photometry in the B (Bergeron et al. 2001) and U band (averages from the compilation of McCook & Sion 1999) is plotted as filled circles. The observations are compared to varied model spectra. LHS 1126: $T_{\rm eff}$ = 5400 K, $\log g$ = 7.9, H/He = 3×10^{-6} (solid line), pure helium (dotted), and H/He = 1×10^{-2} (dashed). LP 658-2: $T_{\rm eff}$ = 5050 K, $\log g$ = 8.3, H/He = 5×10^{-4} (solid), pure helium (dotted). BPM 4729: $T_{\rm eff}$ = 5500 K, $\log g$ = 8.21, H/He = 3×10^{-5} (solid), $T_{\rm eff}$ = 5730 K, $\log g$ = 8.21, pure hydrogen (dotted). All models have been fitted to the V magnitude.

Space Telescope Science Institute and other members of the FOS team and have concluded that the data reduced with the standard FOS pipeline are – to the best of our knowledge – calibrated correctly.

LHS 1126 (WD 0038−226) is one of the few C_2H stars, a spectral class introduced by Schmidt et al. (1995). These objects exhibit broad optical absorption features which have at first been interpreted as blueshifted C_2 Swan

Table 2. Effective temperatures, gravities, and element abundances (by number). The errors include systematic uncertainties and are determined from visual comparisons to model atmospheres. The five hottest objects are of spectral type DBZ(A) and the others of spectral type DZ(A).

Object		$T_{\rm eff}$/K	$\log g$	$\log$ H/He	$\log$ C/He	$\log$ Mg/He	$\log$ Si/He	$\log$ Ca/He	$\log$ Fe/He
vMa 2[a]	1	5700 ± 200	7.9 ± 0.2	-5.0 ± 0.5		-9.1 ± 0.3	<-9.0	-10.65 ± 0.2	-9.4 ± 0.2
L 745-46A[b]	2	7500 ± 200	8.0 ± 0.2	-3.1 ± 0.4	<-8.0	-9.05 ± 0.2	-9.4 ± 0.35	-10.60 ± 0.2	-9.8 ± 0.2
Ross 640[b]	3	8500 ± 200	8.0 ± 0.2	-3.3 ± 0.3	<-9.0	-7.25 ± 0.65	-7.5 ± 0.5	-8.65 ± 0.45	-8.3 ± 0.15
L 119-34[a]	4	9200 ± 300	8.0 ± 0.5	$-4.0^{+0.5}_{-1.0}$	-6.0 ± 0.5	-6.8 ± 0.7	-7.9 ± 0.4	-9.1^{d}	-7.95 ± 0.7
K 789-37[a]	5	$10\,500 \pm 300$	8.0 ± 0.5	-3.8 ± 0.5	<-7.5	-7.6 ± 0.6	-7.5 ± 0.5	-7.9 ± 0.2	-7.4 ± 0.3
GD 408[a]	6	$13\,750 \pm 250$	8.0 ± 0.2^{e}	-6.0 ± 0.3^{e}	$<-7.0^{h}$	-8.5 ± 0.5	<-8.0	-9.6 ± 0.3	$-7.5^{+0.5}_{-1.0}$
HS 2253[c]	7	$14\,700 \pm 500$	8.0 ± 0.25	$-5.0^{+0.7}_{-0.5}$	<-7.5	-5.4 ± 0.2	-5.5 ± 0.7	-6.1 ± 0.4	-5.1 ± 0.1
GD 40[c]	8	$15\,150 \pm 600$	8.0 ± 0.25	-5.3 ± 0.5	-7.2 ± 0.2	-6.0 ± 0.6	-6.5 ± 0.5	-6.7 ± 0.3	-6.2 ± 0.1
GD 378[a]	9	$17\,000 \pm 800$	7.9 ± 0.2^{f}	-4.0^{g}	$<-6.7^{h}$	-6.5 ± 0.8	<-6.5	-8.15 ± 0.5	<-5.5
GD 303[a]	10	$18\,000 \pm 1000$	7.8 ± 0.2^{f}	$<-5.5^{g}$	$<-6.5^{h}$	-5.75 ± 0.5	<-7.0	-7.75 ± 0.5	$-5.5^{+0.5}_{-1.5}$

[a] This paper; [b] Paper I (Koester & Wolff 2000); [c] Friedrich et al. (1999); [d] Zeidler-K.T. et al. (1986); [e] Weidemann & Koester (1991); [f] Oke et al. (1984); [g] Sion et al. (1988); [h] Wegner & Nelan (1987) .

bands. Schmidt et al., however, showed that C_2H is the most probable carbon and hydrogen compound to be formed under the conditions in LHS 1126. The strong infrared flux deficiency reported by Wickramasinghe et al. (1982) could be explained by Bergeron et al. (1994) using collision-induced absorption of H_2 with He.

Bergeron et al. (1997, 2001) have determined $T_{\rm eff} = 5400 \pm 170$ K, $\log g = 7.91 \pm 0.17$, and $\log$ He/H $= 1.86$ from optical/infrared photometry together with the trigonometric parallax. In Fig. 3 we present a model calculation (dashed line) using the parameters from Bergeron et al. and compare it with the HST/FOS spectrum and the photometry. The model flux is significantly too high at infrared wavelengths. This could be expected since we do not include collision-induced absorption in our calculations. More severe is, however, the failure in the ultraviolet. We have included absorption by Lα in the same way as for L 745-46A and Ross 640 (see Sect. 2 and Paper I). The high hydrogen abundance of LHS 1126 results in an extremely strong absorption.

The observed Lα profile can be fitted much better if the abundance is reduced to H/He $= 3 \times 10^{-6}$ (solid line in Fig. 3). Lα absorption is still significant as can be seen from the comparison with a pure helium atmosphere (dotted line). The low hydrogen abundance implied by the ultraviolet flux poses a severe problem since a high value is required to explain the infrared flux deficiency by collision-induced absorption. Our approach to model the Lα wing has been tested successfully at about 2000 K higher effective temperatures. It is possible that this approach fails at lower temperatures although the observed profile can be fitted very well. It could nevertheless be expected that Lα absorption must be strong for an abundance of H/He $\approx 10^{-2}$. However, the observations do not show a strong UV flux deficiency.

A much simpler atmospheric composition is found in LP 658-2 (WD 0552−041) which is classified DZ due to the presence of sharp Ca II lines (Eggen & Greenstein 1965). Bergeron et al. (2001) have fitted the optical and ultraviolet photometry using a pure helium atmosphere with $T_{\rm eff} = 5060 \pm 60$ K and $\log g = 8.31 \pm 0.02$. In Fig. 3 we compare a model (dotted line) with these parameters to the observed flux distribution. The optical and infrared photometry can be reproduced but the ultraviolet part is again unsatisfactory. If the flux deficiency is attributed to the absorption from Lα then about H/He $= 5 \times 10^{-4}$ would be necessary (solid line in Fig. 3). In contrast with LHS 1126, the shape of the absorption feature cannot be reproduced in detail. Higher hydrogen abundances seem to be necessary for $\lambda < 3000$ Å but the absorption at longer wavelengths would then be too strong. Our approach for Lα seems to overestimate the absorption in the outermost wing.

The third cool object with FOS observations is BPM 4729 (WD 0752−676). Wickramasinghe & Bessell (1979) have detected weak Hα and Hβ lines. Bergeron et al. (1997, 2001) could fit the optical/infrared photometry and Hα with $T_{\rm eff} = 5730 \pm 110$ K, $\log g = 8.21 \pm 0.09$, and a pure hydrogen atmosphere. We compare in Fig. 3 a pure hydrogen model (dotted line) to the observed flux distribution. Again, the ultraviolet part where Lα is important cannot be reproduced. The predicted profile for Lα in a *hydrogen* atmosphere is completely at odds with the observation. The ultraviolet part looks more like a helium-dominated atmosphere similar to LHS 1126 or LP 658-2. It is indeed possible to fit this region with H/He $= 3 \times 10^{-5}$ at about $T_{\rm eff} = 5500$ K. However, optical hydrogen lines are not visible under these conditions raising doubts on the validity of this solution.
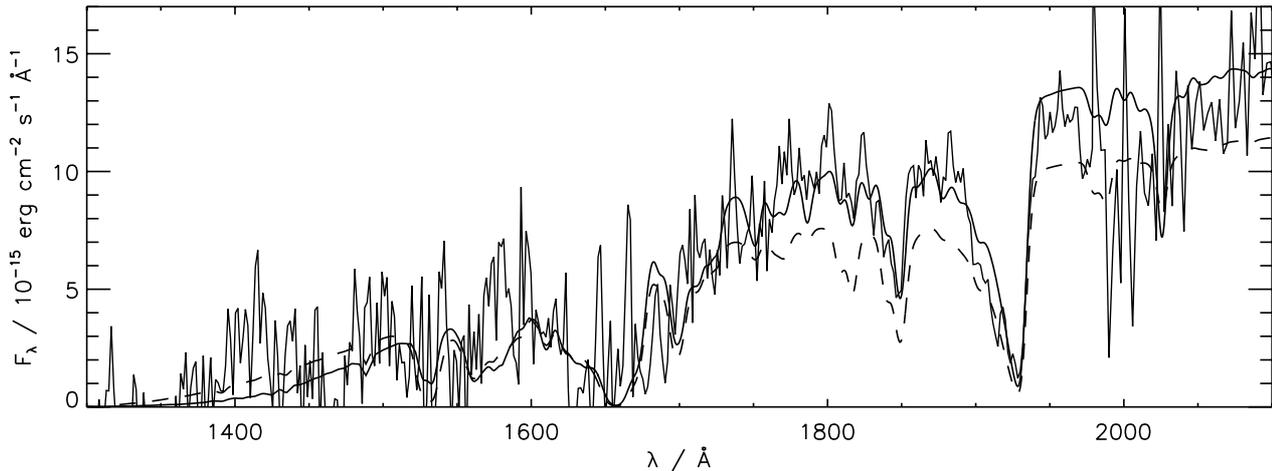
Fig. 4. Lα wing of L 119-34. The thick continuous curve is a model with $T_{\text{eff}} = 9200$ K and $\log \text{H/He} = -4.0$. The dashed curve is a model with $T_{\text{eff}} = 8900$ K; the lower temperature can only partly be compensated by a lower hydrogen abundance ($\log \text{H/He} = -5.0$). The observed spectrum shows also the C I line at 1930 Å, Ca II at 1840 Å, and several Fe II lines.

All three objects presented here show problems if the infrared and ultraviolet parts of the electromagnetic spectrum are to be fitted simultaneously. In LP 658-2, additional absorption, most probably from Lα, seems to be present which would not affect severely the solution from the optical/IR photometry. In LHS 1126 and BPM 4729, however, the ultraviolet and infrared observations require completely different atmospheric compositions. We should note that the HST observations are consistent with existing photometry in the B and U bands which is plotted as filled circles in Fig. 3. Therefore, the discrepancies between the observations and some models cannot be attributed to remaining uncertainties in the FOS calibration.

Bergeron et al. (1997, 2001) have also noted difficulties in fitting the blue energy distribution. They have tried to explain this with a missing opacity, attributed to a pseudo-continuum originating from the Lyman edge, for which no physical discription exists. However, one source of opacity which necessarily is present and which is very strong at cool temperatures is the Lα line. The ultraviolet part of the spectrum is therefore essential for a determination of the H/He ratio. We have shown with our new theoretical discription that at least in He-rich objects the wing extends into the blue part of the optical spectrum. Under these extreme conditions our line profile calculations may be only a first approximation and we cannot yet present satisfactory fits. It seems to be important, however, to consider the whole energy distribution of these objects from the UV to the IR to achieve a correct interpretation.

Bergeron et al. (1997, 2001) draw far-reaching conclusions based on their findings of H/He ratios in cool white dwarfs, e.g. the absence of He atmospheres between 5000 and 6000 K, and their re-appearance below 5000 K. With our demonstration in this paper that the parameters from Bergeron et al. fail to explain the UV flux distribution of several objects it is clear that we have currently not reached a consistent interpretation of these objects. The question of H vs. He atmospheres or the H/He ratio in mixed atmospheres needs further study.

4.3. L 119-34 and K 789-37

L 119-34 (WD 2216−657) and K 789-37 (WD 1225−079) have similar effective temperatures of about 10 000 K. IUE spectra are available for both objects, for K 789-37 we can also use an optical spectrum (3600–5000 Å) obtained with the 1.9m telescope of the South African Astronomical Observatory (Koester et al. 1990). K 789-37 exhibits Hα, Hβ, Mg I, and Ca II in optical spectra. The IUE spectrum adds Mg II, Si I, Fe I, and Fe II. We use the IUE spectrum, the visual magnitude ($V = 14.79$) and the Strömgren colors ($b - y = 0.05$, $u - b = 0.16$) from Kilkenny (1986, 1987) to define the overall flux distribution.

We start the analysis of K 789-37 by investigating the effective temperature and the hydrogen abundance. Since Lα determines the spectral shape at the shortest UV wavelengths both quantities have to be analyzed simultaneously. However, only a rough estimate of the hydrogen abundances is necessary for the temperature determination because Lα depends only weakly on the exact value of the abundance. If we assume $\log g = 8$ we derive $T_{\text{eff}} = 10\,500$ K from a fit to the V magnitude and the IUE spectrum; a visual inspection of Hβ gives $\log \text{H/He} = -3.8$. The Strömgren colors are also compatible with these values: $b - y = 0.09$ and $u - b = 0.16$ for $T_{\text{eff}} = 10\,500$ K. They would, however, favor a somewhat higher temperature of about 11 000 K. We can determine the surface gravity only very inaccurately with the existing data. An estimate is possible due to the different sensitivity of Hβ and Lα to changes in $\log g$ and hydrogen abundance. The effect of a lower or higher gravity on Hβ can be compensated to some extent by the hydrogen abundance but this leads eventually to an incompatible flux at the shortest IUE wavelengths. We estimate a possible range
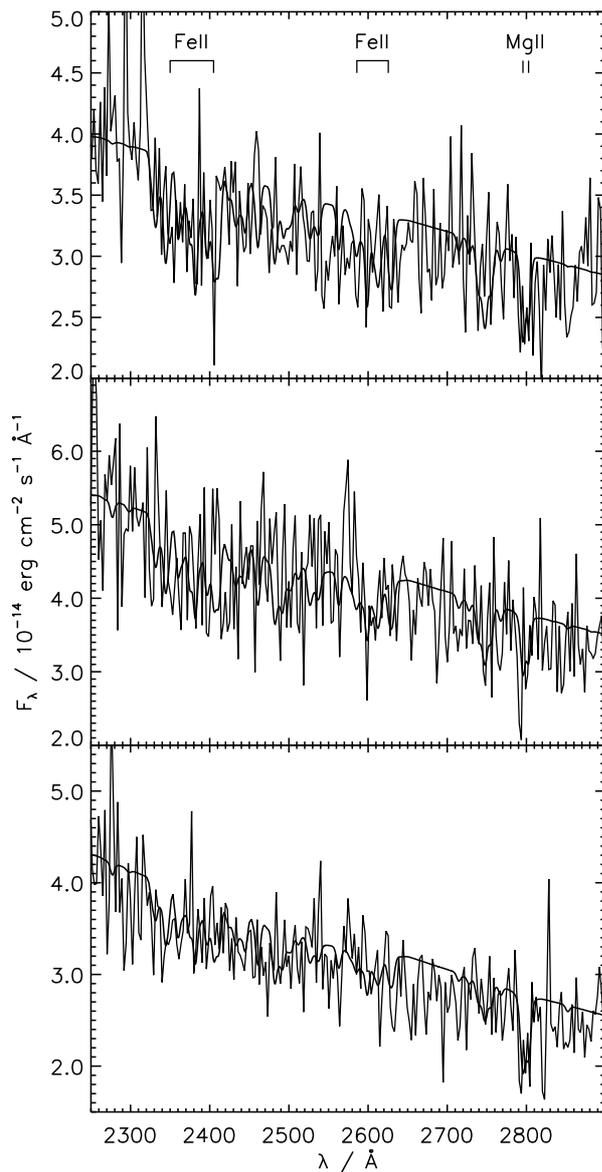
Fig. 5. IUE spectra of GD 408 (top), GD 378 (middle), and GD 303 (bottom) compared with model atmospheres for the parameters of Table 2.

of $\log g = 8.0 \pm 0.5$. The uncertainty of the gravity implies errors of ± 300 K for $T_{\rm eff}$ and ± 0.5 for $\log {\rm H/He}$.

The new effective temperature is about 1000 K higher than the previous results from Liebert et al. (1987; $T_{\rm eff} = 9700$ K) using multichannel spectrophotometry and Koester et al. (1990; $T_{\rm eff} = 9500 \pm 500$ K) using IUE and optical spectra. The latter could reproduce the optical spectrum with 10 000 K whereas the UV flux of the model was too high with this temperature. We attribute these problems to the missing Lα opacity in their models.

For the analysis of the metal lines, we use $T_{\rm eff} = 10\,500$ K, $\log g = 8.0$, and $\log {\rm H/He} = -3.8$. The derived abundances are listed in Table 2. The errors represent the uncertainties in effective temperature and gravity. For magnesium, there are additional uncertainties due to the line profile of the Mg II lines at 2796/2803 Å. The

observed profile cannot be reproduced exactly, a problem which is also known from the analysis of Ross 640 (Paper I). The broadening of the magnesium lines is determined by van-der-Waals interaction with neutral helium. To reproduce the observed profile, we have increased the broadening parameter for van-der-Waals interaction (γ_6) by a factor of five (see also Zeidler-K.T. et al. 1986). We added (quadratically) an additional error of 0.5 dex to account for the uncertainty due to the line profile. The error of the iron abundance represents also the small differences if the abundances are derived from Fe I or Fe II, respectively. The silicon abundance has to be taken with caution because Si I cannot be identified clearly. The same is true for aluminum ($\log {\rm Al/He} = -7.75 \pm 0.5$, not listed in Table 2). From the non-detection of the C I line at 1931 Å, we determine an upper limit of $\log {\rm C/He} = -7.5$.

Contrary to K 789-37, hydrogen lines could not be detected in existing optical spectra of L 119-34, until now (see Zeidler-K.T. et al. 1986). However, the shorter wavelength part of the IUE spectrum indicates strongly the presence of Lα. We, therefore, determine simultaneously effective temperature and hydrogen abundance from the overall flux distribution as given by the IUE spectrum and the visual magnitude ($V = 14.43$, Eggen 1969). This is possible due to the different influence of $T_{\rm eff}$ and Lα on the ultraviolet spectrum. The situation is illustrated in Fig. 4. From a visual comparison we derive $T_{\rm eff} = 9200 \pm 300$ K and $\log {\rm H/He} = -4.0^{+0.5}_{-1.0}$. Since the surface gravity cannot be determined with existing observations we have assumed $\log g = 8.0 \pm 0.5$. This is not critical because the shape of the ultraviolet spectrum depends only weakly on the gravity. The Strömgren colors $b-y$ and $u-b$ (Zeidler-K.T. et al. 1986) can also be used for a temperature estimate. They give $T_{\rm eff} = 9200^{+1000}_{-300}$ K, in agreement with the above value.

The element abundances, as determined from the IUE spectrum, are listed in Table 2. The errors reflect the uncertainties in effective temperature and gravity. For silicon, an additional error of ± 0.2 is added because of the difficulty to reproduce all Si I lines with the same abundance. An additional error of ± 0.25 has also been taken into account for iron because of abundance differences between Fe I and Fe II lines.

4.4. GD 408, GD 378, and GD 303

GD 408 (WD 0002+729), GD 378 (WD 1822+410), and GD 303 (WD 1011+570) are three DBZ stars with effective temperatures well above 10 000 K. Photospheric Ca II lines could be detected in all three objects but other metal determinations do not exist in the literature. We examine the IUE spectra and the optical observations of Sion et al. (1988).

Weidemann & Koester (1991) have determined $T_{\rm eff}$ from multichannel spectrophotometry and $\log g$ with the help of the trigonometric parallax for GD 408. Oke et al. (1984) used multichannel data to determine $T_{\rm eff}$ and $\log g$

for GD 378 and GD 303. We have used the results for the gravity in our analysis but have tested the previous temperature determinations using the IUE spectra and the visual magnitudes. Our results for GD 408 and GD 303 (see Table 2) are compatible with the previous values; for GD 378 we determine a temperature about 1500 K hotter than Oke et al. (1984).

The IUE spectra of all three stars reveal weak lines from Mg II and Fe II (Fig. 5). Since these features are present in all three spectra we are confident that they are not observational artifacts. The derived abundances are listed in Table 2. The errors include uncertainties due to errors in effective temperature and gravity. We have also analyzed the optical spectra of Sion et al. (1988) again. Our new values for the calcium abundance are about two orders of magnitude higher than the values derived by Dupuis et al. (1993b) because the scaling of the equivalent width by the square root of the abundance, as used by Dupuis et al. in their analysis, does not give reliable results here.

5. Discussion

We have analyzed effective temperatures, gravities, and surface abundances for six DZ/DBZ white dwarfs. For the following discussion, we add the results from Paper I and the two DBZ white dwarfs from Friedrich et al. (1999). These ten stars span virtually the complete range of temperatures of DZ/DBZ white dwarfs. They are the only objects with ultraviolet observations which provide the best possibility to investigate the whole spectrum of metals; in optical observations, only Ca II is found in general. We collect the parameters for all stars in Table 2.

We start with a comparison of the observed abundances with the predicted ranges from the model of Dupuis et al. (1993b) in Fig. 6. The two continuous curves in each panel represent the lowest and highest possible abundances at each effective temperature. The lower curves correspond to the equilibrium abundances reached in the low accretion phase ($\dot{M} \approx 5 \times 10^{-20}$ $M_\odot$ yr^{-1} for 49 million years in the model of Dupuis et al.) whereas the upper curves correspond to the maximum abundance reached during passages through interstellar clouds ($\dot{M} \approx 5 \times 10^{-15}$ $M_\odot$ yr^{-1} for one million years). Both curves should be taken with some caution since the actual values of the accretion rates are not known exactly. Moreover, the upper curve depends also partly on the duration of the cloud encounter since an equilibrium between accretion and diffusion is not reached at all temperatures during the assumed passage value of 10^6 years.

The comparison shows that the model assumptions can account in general for the observed metal abundances since most observed values are well between the two limits of the model predictions. Only the observations of GD 40 and HS 2253+8023 (numbers 7 and 8 in Fig. 6) are in part above the upper limits but this can be attributed to the mentioned uncertainties. The data in Fig. 6 seem also to indicate a correlation of the abundances with effective

temperature. This is, however, a selection effect since at higher temperatures only high metal abundances can be detected in the low resolution and low signal-to-noise observations normally used to identify DZ white dwarfs (see e.g. Zeidler-K.T. et al. 1986 for quantitative estimates of the visibility ranges).

Further information about the accretion process can be extracted from the ratios of the metal abundances. Figure 7 shows the values for the six independent combinations of the four observed metals. Again, the continuous curves define the allowed ranges from the model of Dupuis et al. (1993b). The straight line is the solar abundance ratio which is reached in the first moments of a cloud encounter if the accreted material has solar composition. Afterwards, the ratio is altered due to diffusion and approaches the equilibrium value (not shown in Fig. 7) which is always within 0.5 dex of the solar ratio. The second curve in Fig. 7 corresponds to the maximum (or minimum) value reached shortly after a cloud encounter when the abundance of the element with the shorter diffusion time scale is again near the value during low accretion. Afterwards, the ratio turns back to the equilibrium value. At any time, the observed abundance ratio must be between the two curves shown in Fig. 7. The difference between them depends on the diffusion time scales of the two elements.

Most individual abundance ratios fall into the predicted range. They are also often near the solar value (and the equlibrium value) which can be seen well in the Mg/Ca and Fe/Mg diagrams. This implies that we observe the DZ stars mostly during the high accretion phase – in agreement with the observation that the abundances in Fig. 6 are near the upper curve. The deviations from the predicted regions could be attributed to individual variations of the chemical composition of the accreted material which could be different from star to star. However, we follow here the discussion of Dupuis et al. (1993b) who explained these differences by the same changes of the composition for all stars. This conclusion is supported by systematic tendencies which were not clearly present in previous studies: Several observed values especially of the Si/Ca and Si/Fe ratios are below the allowed range.

If the abundance of one element in the accreted material is changed then the whole region of possible ratios in Fig. 7 is shifted by that amount. If we want virtually all measured values to fall into the predicted range then the silicon abundance must be changed by a factor of ≈ 0.2 (-0.7 dex) and the calcium abundance by a factor of ≈ 2 (0.3 dex). Similar values were also determined by Dupuis et al. (1993b).

The underabundance of silicon is interesting in connection with the assumption that metals are accreted onto white dwarfs in the form of grains. Silicon has the lowest condensation temperature of the four metals usually found in DZ spectra (see e.g. Spitzer 1978, Fig. 9.1). During the formation of grains for example in the winds of cool giants it condenses later than the other elements. It has, therefore, a lower depletion factor in the gas phase of the
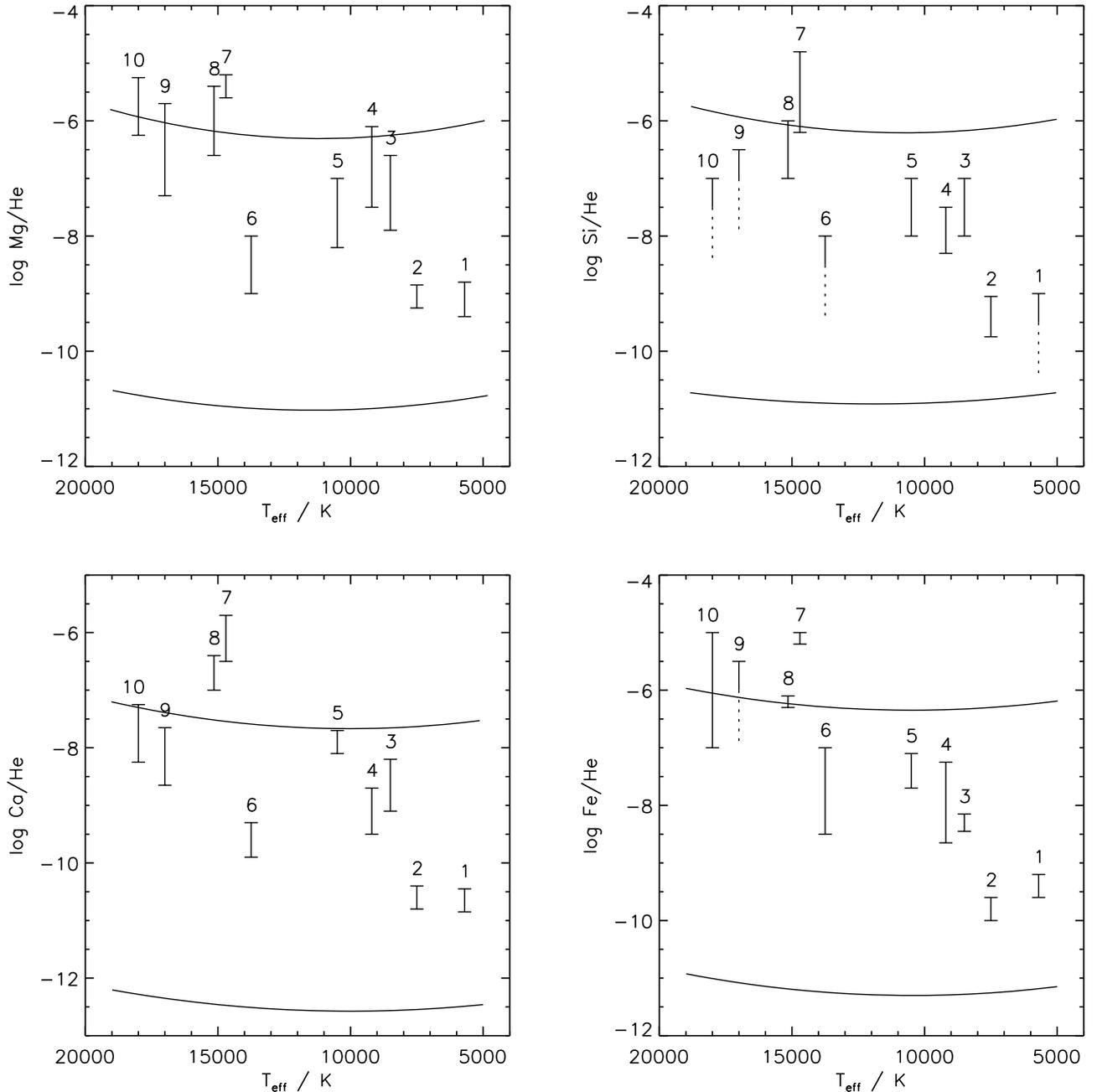
Fig. 6. Observed metal abundances (error bars) compared with the predicted ranges from the two-phase accretion model of Dupuis et al. (1993b). The lower continuous curve is the equilibrium abundance reached in the low accretion phase. The upper curve is the maximum abundance during an encounter with an interstellar cloud. Observational upper limits are denoted by dashed bars. The labels correspond to the numbering in Table 2.

interstellar medium and may be underabundant in the grains accreted onto white dwarfs. During the infall onto the white dwarf silicon could be evaporated earlier than other metals and may partly not reach the surface. Other elements with higher condensation temperatures would survive the accretion process better. Note that calcium, which is probably overabundant, has the highest condensation temperature of the four metals.

In contrast to heavier elements, hydrogen is not accreted in the form of grains. As mentioned in the introduction, it can only be observed in DZ white dwarfs at

unexpectedly low abundances. Nine of our objects exhibit hydrogen, in two of them we could show for the first time its presence through absorption by Lα. The distribution of hydrogen abundances against the effective temperatures of the stars is shown in Fig. 8. As in previous investigations, a correlation with effective temperature cannot be observed. We show as a comparison also the expected hydrogen abundance for continuous accretion of $\dot{M} = 10^{-18}\ M_\odot\ \mathrm{yr}^{-1}$ (Dupuis et al. 1993b). The calculation assumes solar composition of the accreted material and a start of the accretion at $T_{\mathrm{eff}} = 20\,000$ K.
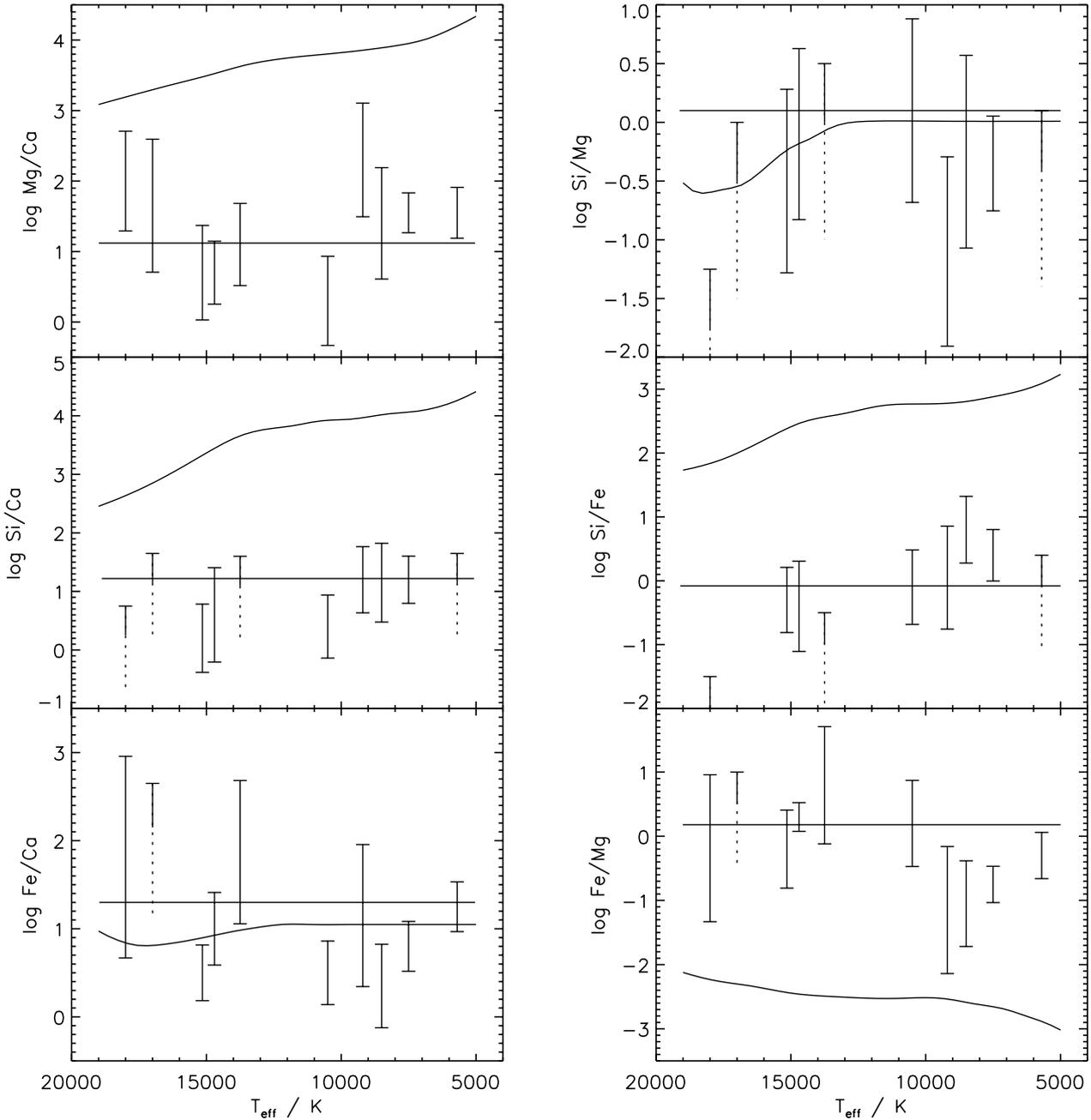
Fig. 7. Observed metal abundance ratios (error bars) compared with the predicted ratios from Dupuis et al. (1993b). The two continuous curves give the possible range if the accreted material has solar composition. Upper limits from the observations are denoted by dashed bars.

The exact choice of the starting point is not critical because of the rapidly increasing cooling ages towards lower temperatures. Figure 8 shows that the actual average accretion rate of hydrogen must be lower than $\dot{M} = 10^{-18}\ M_\odot\ \mathrm{yr}^{-1}$ for our sample objects. On the other hand, the accretion rate for metals – averaged over 5×10^7 years – in the model of Dupuis et al. is about $\dot{M} = 10^{-16}\ M_\odot\ \mathrm{yr}^{-1}$. Therefore, the hydrogen accretion rate is at least two orders of magnitude lower than the metal accretion rate, even for those objects with the highest hydrogen abundances.

In this context, the ratio of hydrogen to other metals is also interesting. Figure 9 shows the observed calcium-to-hydrogen ratios. The weak tendency in temperature which might be observed in the data is due to a similar effect visible in the calcium abundances (see above). Figure 9 shows also the maximum value of Ca/H which can be expected for accretion of material with solar composition within the model of Dupuis et al. (1993b). All observed values are significantly higher than the theoretical upper limit. This shows again that hydrogen is not accreted at solar abundance ratios relative to metals.
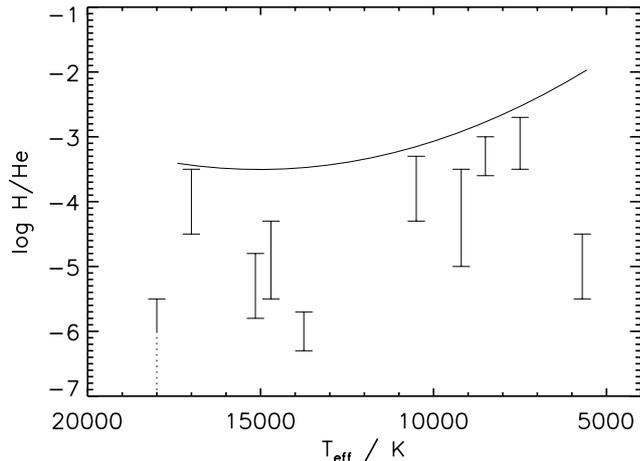
Fig. 8. Observed hydrogen abundances compared to the expected abundance for continuous accretion of material with solar composition with $\dot{M} = 10^{-18} \ M_\odot \ \mathrm{yr}^{-1}$.
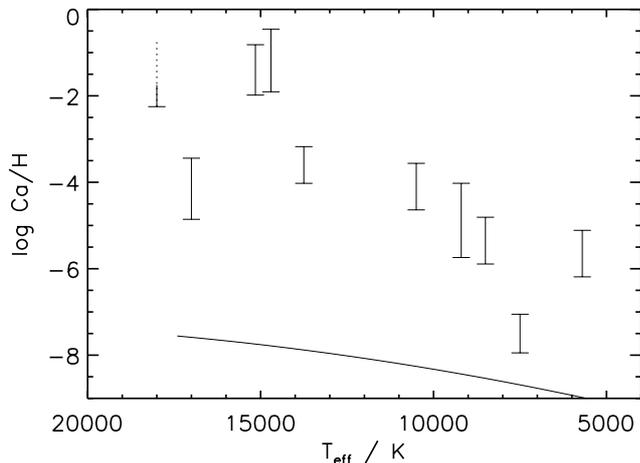

Fig. 9. Calcium-to-hydrogen ratios compared to the maximum Ca/H ratio which could be expected for accretion of material with solar composition.

6. Conclusions

The element abundances of the ten DZ and DBZ white dwarfs presented in this paper form a homogeneous set of data which has been compared to the two-phase accretion model of Dupuis et al. (1993b). The absolute values are in the expected range for accretion from the interstellar medium. Most metal abundance ratios are also compatible with the predictions. Small deviations could be an indication of non-solar metal-to-metal ratios in the accreted material. This tendency is more clearly visible in our improved data set than in the previous investigation of Dupuis et al. (1993b). Hydrogen is present in virtually all of our objects. However, the average accretion rate of hydrogen must be more than two orders of magnitude lower than the average accretion rate of the metals – even in those objects with the highest hydrogen abundances. Therefore, the fate of hydrogen remains unclear.

Our success in modeling Lα absorption in L 745-46A and Ross 640 (Paper I) provides a new means of detecting hydrogen in those cases where the Balmer lines are already very weak. This method has been used to determine the hydrogen abundance in L 119-34 and van Maanen 2. This is important especially for the latter object because Hα is not visible at this combination of effective temperature and hydrogen abundance. In three other white dwarfs with temperatures similar to van Maanen 2 the ultraviolet region of the spectrum indicates a completely different chemical composition than that implied by the optical and infrared photometry. However, we are at the moment not in the position to solve this discrepancy. The analysis of van Maanen 2 shows also that the analysis of optical and infrared photometry can lead to wrong effective temperatures if the absorption by metals in the ultraviolet is not considered. The temperature would be about 1000 K higher without appropriate blanketing in the UV.

References

Allard, N., & Kielkopf, J. 1991, A&A, 242, 133
Bergeron, P., Ruiz, M.-T., Leggett, S. K., Saumon, D., & Wesemael, F. 1994, ApJ, 423, 456
Bergeron, P., Ruiz, M. T., & Leggett, S. K. 1997, ApJS, 108, 339
Bergeron, P., Legget, S. K., & Ruiz, M. T. 2001, ApJS, 133, 413
Dupuis, J., Fontaine, G., Pelletier, C., & Wesemael, F. 1992, ApJS, 82, 505
Dupuis, J., Fontaine, G., Pelletier, C., & Wesemael, F. 1993a, ApJS, 84, 73
Dupuis, J., Fontaine, G., & Wesemael, F. 1993b, ApJS, 87, 345
Eggen, O. J. 1969, ApJ, 157, 287
Eggen, O. J., & Greenstein, J. L. 1965, ApJ, 141, 83
ESA 1997, The Hipparcos and Tycho Catalogues, vols. 1–16 (ESA Publications Division, Noordwijk)
Finley, D. S., Koester, D., & Basri, G. 1997, ApJ, 488, 375
Friedrich, S., Koester, D., Heber, U., Jeffery, C. S., & Reimers, D. 1999, A&A, 350, 865
Grenfell, T. C. 1974, A&A, 31, 303
Kilkenny, D. 1986, Observatory, 106, 201
Kilkenny, D. 1987, MNRAS, 229, 345
Koester, D., & Wolff, B. 2000, A&A, 357, 587 (Paper I)
Koester, D., Wegner, G., & Kilkenny, D. 1990, ApJ, 350, 329
Liebert, J., Wehrse, R., & Green, R. F. 1987, A&A, 175, 173

McCook, G. P., & Sion, E. M. 1999, ApJS, 121, 1

Mihalas, D., Hummer, D. G., Mihalas, B. W., & Däppen, W. 1990, ApJ, 350, 300

Nichols, J. N., Garhart, M. P., de la Peña, M. D., & Levay, K. R. 1994, NASA IUE Newsletter, 53

Oke, J. B., Weidemann, V., & Koester, D. 1984, ApJ, 281, 276

Provencal, J. L., Shipman, H. L., Koester, D., Wesemael, F., & Bergeron, P. 2002, ApJ, in press

Saumon, D., & Chabrier, G. 1994, Phys. Rev. A, 46, 2084

Saumon, D., Chabrier, G., & Van Horn, H. M. 1995, ApJS, 99, 713

Schmidt, G. D., Bergeron, P., & Fegley, B. Jr. 1995, ApJ, 443, 274

Sion, E. M., Aannestad, P. A., & Kenyon, S. J. 1988, ApJ, 330, L55

Spitzer, L. 1978, Physical Processes in the Interstellar Medium (John Wiley & Sons, New York)

Wegner, G. 1972, ApJ, 172, 451

Wegner, G., & Nelan, E. P. 1987, ApJ, 319, 916

Weidemann, V. 1960, ApJ, 131, 638

Weidemann, V., & Koester, D. 1991, A&A, 249, 389

Wickramasinghe, D. T., & Bessell, M. S. 1979, MNRAS, 186, 399

Wickramasinghe, D. T., Allen, D. A., & Bessell, M. S. 1982, MNRAS, 198, 473

Wood, M. A. 1994, in The Equation of State in Astrophysics, ed. G. Chabrier, & E. Schatzman E. (Cambridge University Press), IAU Coll. 147, 612

Zeidler-K.T., E.-M., Weidemann, V., & Koester, D. 1986, A&A, 155, 356